

Corrosion engineering on AlCoCrFeNi high-entropy alloys toward highly efficient electrocatalysts for the oxygen evolution of alkaline seawater

Zhibin Chen, Kang Huang, Bowei Zhang, Jiuyang Xia, Junsheng Wu, Zequn Zhang, and Yizhong Huang

Cite this article as:

Zhibin Chen, Kang Huang, Bowei Zhang, Jiuyang Xia, Junsheng Wu, Zequn Zhang, and Yizhong Huang, Corrosion engineering on AlCoCrFeNi high-entropy alloys toward highly efficient electrocatalysts for the oxygen evolution of alkaline seawater, *Int. J. Miner. Metall. Mater.*, 30(2023), No. 10, pp. 1922-1932. <https://doi.org/10.1007/s12613-023-2624-7>

View the article online at [SpringerLink](#) or [IJMMM Webpage](#).

Articles you may be interested in

Nikhil, Gopal Ji, and Rajiv Prakash, [Hydrothermal synthesis of Zn–Mg-based layered double hydroxide coatings for the corrosion protection of copper in chloride and hydroxide media](#), *Int. J. Miner. Metall. Mater.*, 28(2021), No. 12, pp. 1991-2000. <https://doi.org/10.1007/s12613-020-2122-0>

Ya Wei, Yu Fu, Zhi-min Pan, Yi-chong Ma, Hong-xu Cheng, Qian-cheng Zhao, Hong Luo, and Xiao-gang Li, [Influencing factors and mechanism of high-temperature oxidation of high-entropy alloys: A review](#), *Int. J. Miner. Metall. Mater.*, 28(2021), No. 6, pp. 915-930. <https://doi.org/10.1007/s12613-021-2257-7>

Juan Wang, Li-jun Yang, Xiao-chong Zhao, Pan Yang, Wei Cao, and Qing-song Huang, [Highly efficient nanocatalyst Ni₁Co₉@graphene for hydrolytic dehydrogenation of sodium borohydride](#), *Int. J. Miner. Metall. Mater.*, 28(2021), No. 12, pp. 1976-1982. <https://doi.org/10.1007/s12613-020-2090-4>

Chun-duo Dai, Yu Fu, Jia-xiang Guo, and Cui-wei Du, [Effects of substrate temperature and deposition time on the morphology and corrosion resistance of FeCoCrNiMo_{0.3} high-entropy alloy coating fabricated by magnetron sputtering](#), *Int. J. Miner. Metall. Mater.*, 27(2020), No. 10, pp. 1388-1397. <https://doi.org/10.1007/s12613-020-2149-2>

Hong-mei Zhang, Yan Li, Ling Yan, Fang-fang Ai, Yang-yang Zhu, and Zheng-yi Jiang, [Effect of large load on the wear and corrosion behavior of high-strength EH47 hull steel in 3.5wt% NaCl solution with sand](#), *Int. J. Miner. Metall. Mater.*, 27(2020), No. 11, pp. 1525-1535. <https://doi.org/10.1007/s12613-020-1978-3>

Bo-ren Ke, Yu-chun Sun, Yong Zhang, Wen-rui Wang, Wei-min Wang, Pei-yan Ma, Wei Ji, and Zheng-yi Fu, [Powder metallurgy of high-entropy alloys and related composites: A short review](#), *Int. J. Miner. Metall. Mater.*, 28(2021), No. 6, pp. 931-943. <https://doi.org/10.1007/s12613-020-2221-y>



IJMMM WeChat



QQ author group

Corrosion engineering on AlCoCrFeNi high-entropy alloys toward highly efficient electrocatalysts for the oxygen evolution of alkaline seawater

Zhibin Chen¹⁾, Kang Huang¹⁾, Bowei Zhang^{1),✉}, Jiuyang Xia¹⁾, Junsheng Wu^{1),✉}, Zequn Zhang¹⁾, and Yizhong Huang^{2),✉}

1) Institute for Advanced Materials and Technology, University of Science and Technology Beijing, Beijing 100083, China

2) School of Materials Science and Engineering, Nanyang Technological University, Singapore 639798, Singapore

(Received: 13 November 2022; revised: 5 March 2023; accepted: 6 March 2023)

Abstract: Seawater splitting is a prospective approach to yield renewable and sustainable hydrogen energy. Complex preparation processes and poor repeatability are currently considered to be an insuperable impediment to the promotion of the large-scale production and application of electrocatalysts. Avoiding the use of intricate instruments, corrosion engineering is an intriguing strategy to reduce the cost and presents considerable potential for electrodes with catalytic performance. An anode comprising quinary AlCoCrFeNi layered double hydroxides uniformly decorated on an AlCoCrFeNi high-entropy alloy is proposed in this paper via a one-step corrosion engineering method, which directly serves as a remarkably active catalyst for boosting the oxygen evolution reaction (OER) in alkaline seawater. Notably, the best-performing catalyst exhibited oxygen evolution reaction activity with overpotential values of 272.3 and 332 mV to achieve the current densities of 10 and 100 mA·cm⁻², respectively. The failure mechanism of the obtained catalyst was identified for advancing the development of multicomponent catalysts.

Keywords: corrosion engineering; oxygen evolution reaction catalysts; layered double hydroxides; seawater splitting; failure mechanism

1. Introduction

Renewable and eco-friendly energy is required to build a sustainable energy system for mitigating the global energy and pollution issue due to the unrestrained consumption of fossil fuels [1–2]. Hydrogen (H₂) is admittedly regarded as a desired fuel for the green circulation economy due to its significantly high energy density and nontoxic exhaust products in the energy conversion process [3]. Among various technologies for hydrogen production, water electrolysis, which converts water into hydrogen and oxygen products, is a feasible option to achieve an energy landscape in the future and avoids the emission of noxious gas [4–6]. Moreover, the popularization of freshwater electrolysis might be impeded due to the extreme lack of freshwater resources and result in controversies in hot arid regions. Therefore, ocean seawater, which represents 96.5vol% of the total water resources of earth, is assumed to be the almost inexhaustible natural resource and highly suitable electrolyte feedstock for hydrogen products via electrolysis, stimulating an urgent pursuit for the development of cost-efficient seawater electrolysis [7–9]. Governed by the electrochemical reactions, water splitting is divided into hydrogen evolution reaction (HER) and oxygen evolution reaction (OER) for H₂ and O₂ occurrences on the cathode and anode, respectively. Therein, OER is generally

regarded as the bottleneck of water electrolysis because of its multiple proton-coupled electron transfer process and more sluggish intrinsic kinetics than HER, leading to large overpotential and additional energy loss in water electrolysis [10–11]. In comparison with freshwater electrolysis, the challenges of electrochemical seawater splitting, such as low conversion efficiency of H₂ caused by chlorine evolution reaction (CER) [12–13], the aggressive Cl⁻ existing in the seawater [14–15], and insoluble precipitates produced by the dramatic fluctuations of local pH [16], would ruin and block the electrode and lead to poor electrocatalytic activity as well as unsatisfactory stability during electrolysis. Through the effort of many researchers, feasible strategies to address the above-mentioned challenges and realize OER-selective seawater splitting could be summarized as follows: (i) utilizing stable electrocatalysts to decrease the required overpotential for OER, which is considered to be the major strategy for high-efficiency water electrolysis, and (ii) alkalizing the seawater electrolyte, which not only increases the concentration of ions in seawater and prevents drastic fluctuation in local pH but also provides 480 mV of the potential difference between OER and CER in thermodynamics [11–16]. Nevertheless, complex catalysts could not be fabricated in a single step with the emergence of a variety of catalysts for OER. Therefore, an urgent demand for a simple and convenient

✉ Corresponding authors: Bowei Zhang E-mail: bwzhang@ustb.edu.cn; Junsheng Wu E-mail: wujs@ustb.edu.cn; Yizhong Huang E-mail: YZHuang@ntu.edu.sg

preparation method of catalysts is required to reduce the preparation period and cost of multicomponent or complicated catalysts.

Over the past decades, the most commonly employed routes for catalysts are hydrothermal [17–19], solvothermal [20–21], co-precipitation [22–23], electrodeposition [24–25], cation exchange [26–27], and cathode plasma electrolytic deposition [28–29]. However, it is difficult to satisfy the requirements of several multicomponent catalysts generated from complicated reaction systems, including considerable reproducibility, controllability, and practicability for industrial manufacture and commercial applications [30]. In recent years, metal corrosion, which spontaneously and inevitably caused considerable damage to metallic materials in the natural environment, is unexpectedly identified as a simple, reproducible, and low-cost procedure for the large-scale application to *in-situ* preparation of catalytic products onto substrate and minimization of the labor cost and assembly complexity. Benefiting from *in-situ* growth and general 2D/3D structures of products, catalysts produced via the corrosion process would exhibit remarkable conductivity and large active surface area, which is referred to as corrosion engineering, and demonstrated a potential route to generate binder-free, additive-free, and conductive electrodes with remarkable electrocatalytic activities [31–33]. Corrosion engineering has been widely used for simple Ni-, Fe-, and NiFe-based catalysts directly grown onto Ni foam, Fe foam, and stainless steels, respectively. However, corrosion engineering should be continuously explored to produce multicomponent and complicated catalysts [34–38]. Since the realization of electrochemical catalysis in the early days, noble metal-based materials invariably represent the commercial and most effective catalysts (for example, platinum-based materials for HER and ruthenium or iridium oxides for OER) [39–41]. Nevertheless, due to the drawbacks of scarcity on earth and the high cost of commerce, the rapid development and commercial application of precious metal-based catalysts are restricted [42–43]. To date, transition metal-based catalysts, such as relevant sulfides [44–45], phosphides [46–47], nitrides [48], oxides [49], and hydroxides [50], have exhibited remarkable catalytic performance, even surpassing activities of noble metal-based catalysts in many reports [51–53]. Specifically, among various electrocatalytic materials, transition metal-based layered double hydroxides (LDHs) have recently drawn considerable attention owing to numerous advantages, such as unique lamellar structure, tunable chemical composition, large surface area, and structural stability, thus making them an outstanding catalyst for alkaline and neutral electrolysis with low cost and adequate resources [54–58]. Additionally, multicomponent transition metal-based LDHs prepared by incorporating or doping methods would generally further boost the intrinsic kinetics of OER due to the synergistic effect of transition metals [59–60]. Strasser *et al.* [14] firstly reported the remarkable electrocatalytic performance of NiFe-LDHs material in a weak alkaline stimulated seawater (0.1 M KOH + 0.5 M NaCl), realizing 100% Faraday efficiency toward OER and showing the potential of transition metal-based LDHs materials for electrochemical seawater

splitting. Furthermore, as mentioned in several references, *in-situ* formed hydroxide layers on the anode surface play an important role in the service life of catalysts due to the resistance of hydroxide layers for blocking the invasion of Cl⁻ into effective catalytic sites to poison catalyst [9,11,13]. The high-entropy alloys (HEAs) are supposed to be the desirable materials for catalysts to reduce the cost of labor and time during the fabrication of multi-element metal-based catalysts. Significantly, the HEAs exhibit the potential to supply multiple elements simultaneously due to the coexistence feature of multiple elements in one structure, avoiding the addition of metal salts or binders during the fabrication for catalysts directly serving as electrodes toward water splitting. Moreover, the HEAs are assumed to be a promising and functional catalyst material in electrocatalysis due to the synergistic effect of multiple elements adjacent to each other, leading to the formation of new and tailorable active sites [61–63]. Some HEAs with certain components and several high-entropy metallic oxides/hydroxides/phosphates on the surface of HEAs have been verified to possess considerable catalytic performance for water splitting [64–66]. Moreover, most of the HEAs show excellent corrosion resistance and mechanical strength due to special features, including severe lattice distortion, slow diffusion, and high entropy of mixing and unique cocktail effects. Thus, HEAs have tremendous potential to be re-used for catalysis or electrocatalysis with super long service life [67]. Nevertheless, searching for a single-step and large-scale applied fabrication strategy is urgent and indispensable for the commercial application of transition metal-based LDHs catalysts.

In this work, the transition metal-based AlCoCrFeNi quinary LDH (AlCoCrFeNi-LDHs) array *in-situ* grown on an AlCoCrFeNi-HEAs was prepared using the hydrothermal method, in which NaOH and heat drive corrosion process occurred on the surface, and developed as a high-efficiency catalyst for OER in alkaline seawater electrolyte. The conductive substrate of HEAs not only provides metallic ions for LDHs but also serves as the anode of the electrolyzer. HEAs have been verified to possess considerable potential in catalysis [68–70]. Specifically, the influence of heating temperature and solution on morphology and electrocatalytic performance was studied. The major factor that causes the degradation of the OER activity of the AlCoCrFeNi-LDHs catalyst was further investigated. This work provides not only a facile, scalable, and efficient approach to fabricate multi-metal-based LDHs but also a failure mechanism and possible researchful orientation for prolonging the operating life of multicomponent LDH-based catalysts.

2. Experimental

2.1. Fabrication of AlCoCrFeNi-LDHs

The pure Al, Co, Cr, Fe, and Ni metals with high purity (99.99wt%) were obtained by arc melting under an argon atmosphere. Subsequently, the melting and casting of metals were conducted under the vacuum condition of 1 kPa, followed by sweeping with argon three times. The mixture of

raw materials (Table S1) was repeatedly melted and solidified several times to obtain an AlCoCrFeNi-HEAs with a highly alloyed state and ideal chemical homogeneity. AlCoCrFeNi-LDHs were prepared through a facile and one-step hydrothermal approach in a NaOH solution. Firstly, a small piece of AlCoCrFeNi-HEAs with the dimensions of 10 mm × 10 mm × 0.5 mm was ground and thoroughly rinsed with deionized water to remove impurities on the surface of the AlCoCrFeNi-HEAs. Subsequently, the AlCoCrFeNi-HEAs was dried at 60°C under vacuum for 12 h. In a typical preparation procedure, 0.06 mol NaOH was dissolved in 20 mL of deionized water. The above solution and the clean AlCoCrFeNi-HEAs were transferred to a Teflon-sealed autoclave after vigorous stirring. Finally, the autoclave was heated for 8 h at 150°C, followed by cooling to room temperature for AlCoCrFeNi-LDHs to facilitate its growth on the surface of the AlCoCrFeNi-HEAs. The resultant product washed with deionized water and ethanol to remove the residue on the surface, and then dried at 60°C under vacuum for further test, and it was labeled as LDHs-*x* M-*y* h (*x* and *y* correspond to the concentration of NaOH and the duration of heat, respectively).

2.2. Characterization

The morphology and microstructure characterizations were performed by scanning electron microscopy (SEM, Regulus 8100) and transmission electron microscopy (TEM, TECNAI F20), and energy dispersive spectroscopy (EDS) data were also achieved on SEM and TEM microscopes. Grazing incident X-ray diffraction (XRD, Bruker D8 ADVANCE) was conducted to identify the crystallographic structure of the AlCoCrFeNi-LDHs and AlCoCrFeNi-HEAs using the following parameter: Cu K_α radiation, scanning rate of 5°·min⁻¹, and 2θ angle ranging from 10°–90°. X-ray photoelectron spectroscopy (XPS) was performed on a Thermo ESCALAB 250XI, and all data of the binding energy were calibrated to the C 1s peak at 284.8 eV. The content of metal ions was investigated by an inductively coupled plasma-optical emission spectroscopy (ICP-OES), which was performed by using an Agilent ICPOES730.

2.3. Electrochemical measurements

All electrochemical performances were measured on an electrochemistry workstation (Autolab PGSTAT 302N) in stimulated alkaline seawater (1 M KOH + 0.5 M NaCl) at room temperature by a three-electrode configuration. The as-prepared AlCoCrFeNi-LDHs on AlCoCrFeNi-HEAs, graphite rod, and Ag/AgCl saturated KCl served as the working, counter, and reference electrodes, respectively. All potentials

(*E*) were converted to the reversible hydrogen electrode (*E*_{RHE}) according to the formula:

$$E_{\text{RHE}} = E_{\text{Ag/AgCl}} + 0.197 + 0.059 \times \text{pH} \quad (1)$$

The OER activity was exhibited by linear sweep voltammetry (LSV) curves, which were realized at a scan rate of 10 mV·s⁻¹. Additionally, all the LSV curves in this work were corrected with *iR* compensation (80%), and overpotential (*η*) was calculated via the formula:

$$\eta = E_{\text{RHE}} - 1.23 \quad (2)$$

The frequency range of 0.01 Hz to 100 kHz was applied to electrochemical impedance spectroscopy (EIS) measurements, and the numerical relationship of electrochemical surface area (ECSA) of processed samples was evaluated by fitting the value of double-layered capacitance (*C*_{dl}). Meanwhile, the *C*_{dl} value was estimated by cyclic voltammetry (CV) curves in the non-Faradaic potential range at the scan rate of 10, 30, 50, 70, 90, and 110 mV·s⁻¹. The differences in charging current densities (*j* = *j*_a - *j*_c) were linear with the scan rate and the half value of the relevant slope corresponds to the *C*_{dl}. The *i-t* curve stability test of the as-prepared catalyst was conducted at a constant current density of 100 mA·cm⁻² at room temperature. Moreover, the OER performance of the catalyst was measured again after a stability test to contrast the electrochemical activity with an intact catalyst.

3. Results and discussion

The schematic illustration of the preparation process for the AlCoCrFeNi quinary LDH (AlCoCrFeNi-LDHs) catalyst is presented in Fig. 1. Under different NaOH concentrations, the hydrothermal reaction of AlCoCrFeNi-HEAs was conducted at 150°C for different treatment time (including heating up and holding processes) of 4, 8, 12, and 24 h. AlCoCrFeNi-HEAs occurs corrosion during the hydrothermal reaction, followed by the release of five metallic ions combined with OH⁻ to form uniform AlCoCrFeNi-LDHs sheets with high surface area on the HEAs surface. SEM and TEM images were used for the time- and concentration-dependent evolutions of AlCoCrFeNi-LDHs to investigate the growth mechanism, respectively. Fig. 2(a) and S1 reveal the morphology of AlCoCrFeNi-LDHs changes from small and irregular flakes to large and regular sheets, as the concentration of NaOH increases while the heating duration is 8 h. Fig. S1(a) shows the coexistence of tiny LDH flakes and similar-sized metallic oxide particles on the surface of the LDHs-0.1 M-8 h sample. Fig. S1(b) reveals the morphology of sample prepared in 1 M NaOH was a scene of interlaced LDH sheets with different sizes. Subsequently, AlCoCrFeNi-LDH sheets

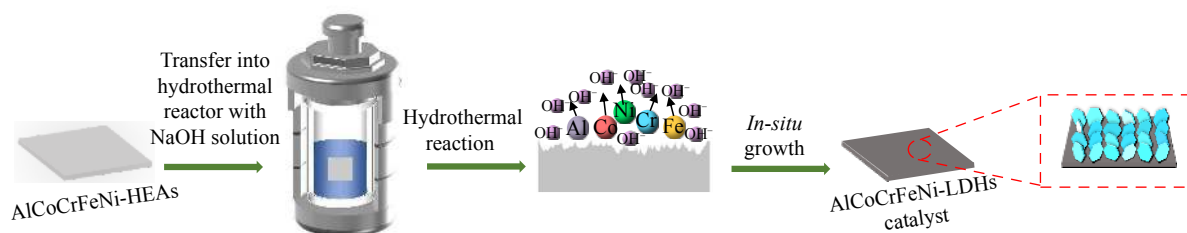


Fig. 1. Schematic illustration of self-supported AlCoCrFeNi-LDHs.

were grown on the surface of the AlCoCrFeNi-HEAs, creating uniform layered structures with large active areas and smooth surfaces after the hydrothermal reaction in 3 M and 5 M NaOH, as shown in Fig. 2(a) and Fig. S1(c), respectively. However, the high concentration (Fig. S1(d–e)) and long hy-

drothermal duration (Fig. S2(b–c)) would lead to the appearance of tablet-shape LDH products in concentration- and time-dependent evolutions, respectively. Moreover, *in-situ* growth of LDHs was proven by the sectional SEM image (Fig. S3).

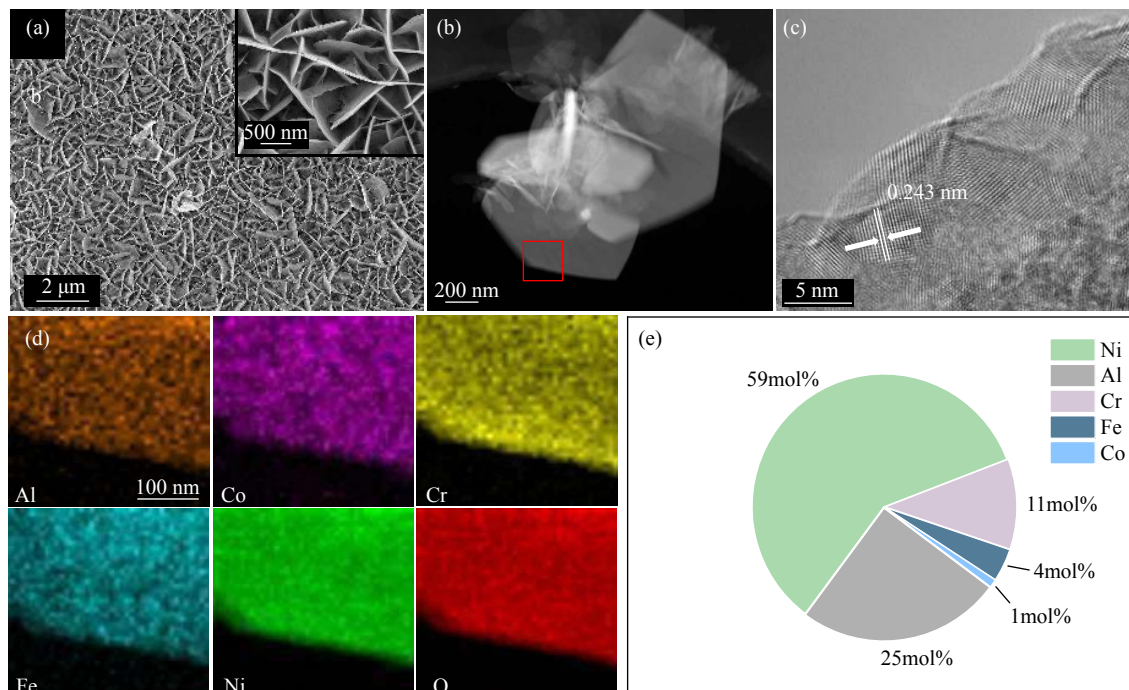


Fig. 2. Microscopic characterization and metallic elemental content of the as-prepared catalyst: (a) SEM image of LDHs-3 M-8 h sample; (b) TEM and (c) HRTEM images of LDH sheets detached from LDHs-3 M-8 h sample, respectively; (d) corresponding elemental mapping of the selected area in (c); (e) elemental content of LDH sheets from LDHs-3 M-8 h sample.

TEM image of the LDH sheets further confirm the extremely thin construction of AlCoCrFeNi-LDHs (Fig. 2(b)), which is consistent with the SEM results. Moreover, lattice fringes with a d -spacing of 0.243 nm were observed in a high-resolution TEM image (Fig. 2(c)), corresponding to the (101) plane. Fig. 2(d) further displays the homogeneous distribution of Al, Co, Cr, Fe, and Ni in the LDH sheets. This finding verifies the successful preparation of quinary LDHs, which are formed by the coinstantaneous incorporation of metallic ions with OH^- . ICP analysis was conducted for the atomic ratio of metals in as-synthesized LDHs and reveals that the atomic ratio of Al, Co, Cr, Fe, and Ni is 1:0.04:0.44:0.16:2.36, as shown in Fig. 2(e).

The XRD analysis was applied to study the crystal structure and phase compositions of the pretreated HEAs and AlCoCrFeNi-LDHs. According to the measurement results of XRD, the existing XRD standard cards (PDF# 06-0696 and PDF# 14-0117) were used as the approximate peak of AlCoCrFeNi-HEAs and AlCoCrFeNi-LDHs. The XRD pattern of the AlCoCrFeNi-LDHs after hydrothermal treatment comprehensively indicates six diffraction peaks at 19.5° , 33.4° , 39.0° , 44.5° , 64.8° , and 82.2° , which are indexed as (001), (100), and (101) planes of the synthesized materials and (110), (200), and (211) planes of AlCoCrFeNi-HEAs substrate (Fig. 3). The chemical compositions and the surface chemical states of the selected catalyst were identified by XPS measurement. The XPS survey spectrum (Fig. 4(a)) re-

veals the presence of Al, Co, Cr, Fe, and Ni along with O elements in the LDH material, consistent with the EDX results (Fig. 2(e)). Fig. 4(b) shows the two peaks at 73.9 and 68.6 eV corresponds to Al 2p and Ni 3p, respectively [71]. The Co 2p spectra (Fig. 4(c)) exhibits two broad peaks assigned as Co 2p_{3/2} and Co 2p_{1/2} at 780.9 and 795.9 eV, respectively. In addition, two additional peaks at 784.3 eV and 799.2 eV correspond to the satellite peaks [72]. Four peaks are found with the high-resolution XPS spectrum of Cr 2p (Fig. 4(d)), including two peaks of Cr 2p_{3/2} and Cr 2p_{1/2} at 577.1 and 586.8 eV, respectively, which are assigned to trivalent chromium hydroxide. The other two tiny peaks at 589.1 and 579.3 eV are reported to be trivalent chromium combined with additional ligands to form complex compounds, which exist on the surface of the catalyst [73]. For the Fe 2p XPS spectrum (Fig. S4(d)), the signals situated at 711.9 and 724.5 eV are related to the Fe 2p_{3/2} and Fe 2p_{1/2}, respectively, denoting the state of Fe³⁺. The peak located at 721.2 eV can be identified as the relevant satellite peak of Fe [9,26]. As shown in Fig. 4(e) for the Ni 2p XPS spectrum, two main peaks of Ni 2p_{3/2} and Ni 2p_{1/2} appear at 856 and 873.3 eV, respectively, as well as two relevant satellite peaks at 861.8 and 879.6 eV, confirming the presence of Ni²⁺ [74]. The XPS spectra of O 1s (Fig. 4(f)) show three peaks located at 531.5, 529, and 533.3 eV, which can be attributed to OH⁻, M–O, and H₂O on the sample surface, respectively.

The electrocatalytic OER activity of the AlCoCrFeNi-

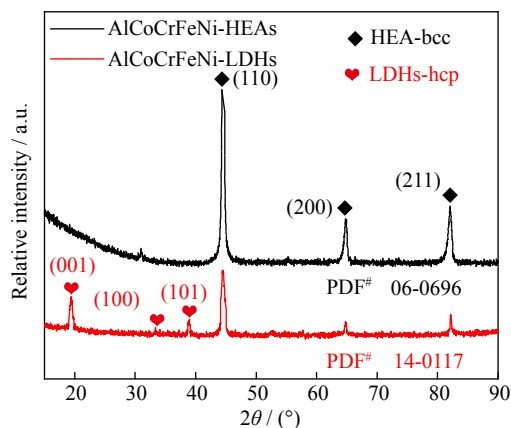


Fig. 3. XRD patterns of AlCoCrFeNi-HEAs and AlCoCrFeNi-LDHs.

HEAs and the as-prepared catalysts with different preparation conditions were evaluated using a standard three-electrode configuration in an alkaline simulated seawater electrolyte (0.5 M NaCl + 1 M KOH) at room temperature. The 0.5 M NaCl solution is generally regarded as an artificial substitute approximately served as natural seawater because of the similar existence of predominant Na^+ and Cl^- [75]. The LSV profiles (Fig. 5(a, d)) showed that LDHs-3 M-8 h exhibits optimal OER activity among all related products and untreated AlCoCrFeNi-HEAs, requiring overpotentials of 272.3 and 332 mV to deliver 10 and 100 $\text{mA}\cdot\text{cm}^{-2}$, respectively. These overpotentials are relatively smaller than LDHs-0.1 M-8 h (326.3 and 418 mV), LDHs-1 M-8 h (301.8 and 383.6 mV), LDHs-5 M-8 h (279.1 and 369 mV), LDHs-7 M-8 h (296.8 and 389.2 mV), LDHs-3 M-4 h (286.3 and 364.9 mV), LDHs-3 M-12 h (290.9 and 368.4 mV), LDHs-3 M-24 h (315.8 and 601.3 mV), and AlCoCrFeNi-HEAs (349.8 and 455.4 mV) to attain the same current densities of 10 and 100 $\text{mA}\cdot\text{cm}^{-2}$. This finding demonstrates that

as-synthesized AlCoCrFeNi quinary LDHs exert a positive influence on electrochemical performance. Notably, the OER activity of the LDH catalyst rises as a function of increased concentration of NaOH or hydrothermal duration from 0 to 3 M or 0 to 8 h, respectively, due to the increasing active site on the surface according to the SEM results (Figs. S1–S2). Oppositely, the electrochemical performance of OER declined gradually with the further increase in concentration or duration due to blocked mass transfer caused by large-sized LDHs. Furthermore, the Tafel plots are displayed in Fig. 5(b, e) to evaluate the catalytic kinetics of the samples for OER. LDHs-3 M-8 h yields a lower Tafel slope of $48.87\text{ mV}\cdot\text{dec}^{-1}$ in comparison with that of LDHs-0.1 M-8 h ($50.25\text{ mV}\cdot\text{dec}^{-1}$), LDHs-1 M-8 h ($50.21\text{ mV}\cdot\text{dec}^{-1}$), LDHs-5 M-8 h ($54.43\text{ mV}\cdot\text{dec}^{-1}$), LDHs-7 M-8 h ($54.9\text{ mV}\cdot\text{dec}^{-1}$), LDHs-3 M-4 h ($53.52\text{ mV}\cdot\text{dec}^{-1}$), LDHs-3 M-12 h ($53.2\text{ mV}\cdot\text{dec}^{-1}$), and LDHs-3 M-24 h ($90.78\text{ mV}\cdot\text{dec}^{-1}$), revealing the relatively rapid OER catalytic kinetics on LDHs-3 M-8 h. Electrochemical impedance spectroscopy (EIS) measurements were employed to determine the charge transfer resistance (R_{ct}) of catalysts, and the Nyquist plots of as-prepared catalysts are presented in Fig. 5(c, f). LDHs-3 M-8 h possess the smallest diameter of the impedance arc among all the samples, demonstrating the smallest R_{ct} and best conductivity, which proves the relatively outstanding catalytic performances. Additionally, the values of C_{dl} , which are measured via CV with increasing scan rate (Figs. S5–S6), were fitted to estimate the electrochemically active surface area. Fig. 5(g–h) shows the C_{dl} values of LDHs-3 M-8 h, LDHs-0.1 M-8 h, LDHs-1 M-8 h, LDHs-5 M-8 h, LDHs-7 M-8 h, LDHs-3 M-4 h, LDHs-3 M-12 h, and LDHs-3 M-24 h were 1.47, 0.53, 1.4, 1.27, 0.8, 1.19, 1.31, and 1.2 $\text{mF}\cdot\text{cm}^{-2}$, suggesting that LDHs-3 M-8 h provides a large surface for active sites during OER and comprises the conclusion of the overpotential mentioned above, and the rel-

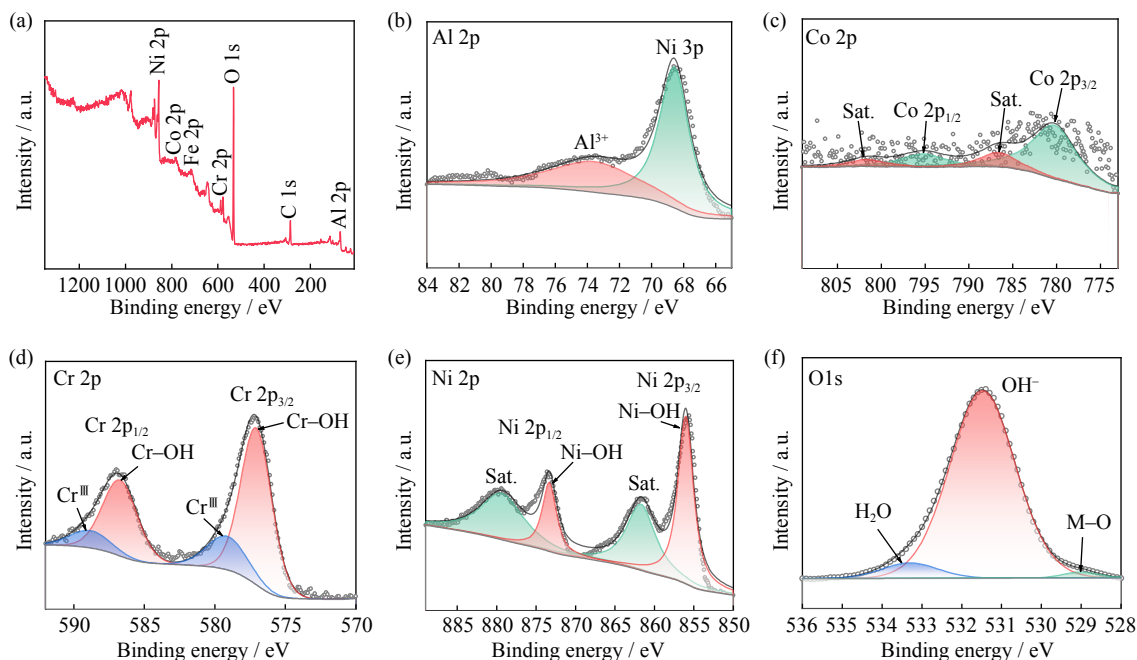


Fig. 4. XPS spectra of LDHs-3 M-8 h: (a) survey spectra; (b) Al 2p; (c) Co 2p; (d) Cr 2p; (e) Ni 2p; (f) O 1s.

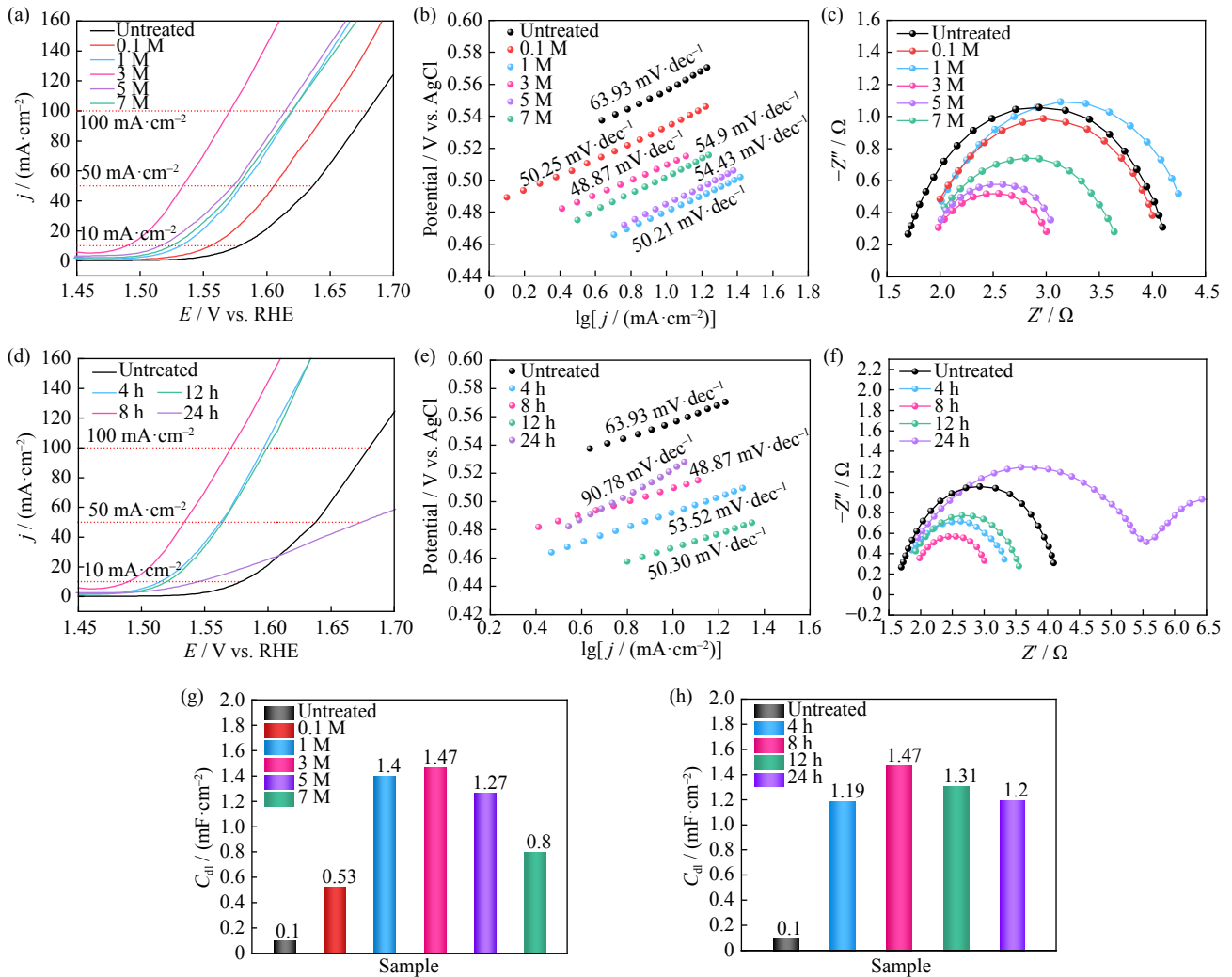


Fig. 5. Electrochemical performance of different samples: AlCoCrFeNi-HEAs, LDHs-0.1 M-8 h, LDHs-1 M-8 h, LDHs-3 M-8 h, LDHs-5 M-8 h, LDHs-7 M-8 h, LDHs-3 M-4 h, LDHs-3 M-12 h, and LDHs-3 M-24 h: (a, d) OER polarization curves in 0.5 M NaCl + 1 M KOH solution; (b, e) corresponding Tafel slope; (c, f) Nyquist plots of different samples; (g-h) C_{dl} values.

ative CV data were displayed in Figs. S5–S6. Based on previous studies, the enhanced electrochemical performance of surface-modified AlCoCrFeNi-HEAs for OER could be concluded as follows: (i) doping effect of transition metal elements for driving synergism and boosting OER kinetics; (ii) unique 2D structure for large electrochemical surface area and substantially exposed active sites; (iii) fast mass transfer and the release of gaseous product due to appropriate space among LDHs sheets; (iv) fast electron transfer speed due to the *in-situ* growth of LDH sheets onto the HEAs electrode [76–82]. Additionally, the OER stability was tested under a constant overpotential for 72 h to evaluate the potential for practical application. Impressively, LDHs-3 M-8 h exhibited excellent performance in successive 24 h at a current density of 100 mA·cm⁻² (Fig. 6). However, the significant fluctuations were found after the following 30 h, and the catalyst underwent a slow but continuous degradation of catalytic performance after the next 18 h. Moreover, the OER activity of the selected LDHs-3 M-8 h catalyst outperforms many recently reported multicomponent-based OER catalysts, and some details are shown in Table 1.

The sample of LDHs-3 M-8 h underwent 72 h stability

test was investigated by the same analysis method to examine the failure mechanism for the degradation of AlCoCrFeNi-LDHs catalysts during the OER electrocatalytic process. Samples of LDHs-3 M-8 h before and after the 72 h stability test are named AlCoCrFeNi-LDHs-BST and AlCoCrFeNi-LDHs-AST, respectively. AlCoCrFeNi-LDHs-AST ex-

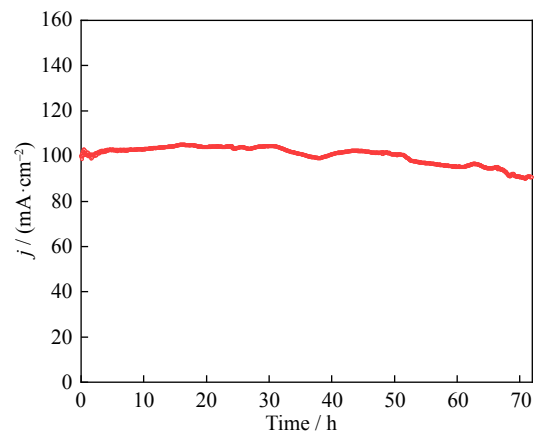


Fig. 6. Stability test of LDHs-3 M-8 h sample for 72 h.

hibited the overpotential of 283 and 364 mV at 10 and 100 mA·cm⁻² (Fig. 7(a)), a high value of the Tafel slope (78.5 mV·dec⁻¹) (Fig. 7(b)), and a relatively large R_{ct} , indicating a

slight degradation of activity for OER than AlCoCrFeNi-LDHs-BST (Fig. 7(c)). However, AlCoCrFeNi-LDHs-AST possessed substantially larger C_{dl} (4.61 mF·cm⁻²) than Al-

Table 1. OER performance of the catalyst in this work in comparison with other multicomponent-based catalysts

Catalyst	Electrolyte	Overpotential / mV	Durability	Ref.
AlCoCrFeNi-LDHs@AlCoCrFeNi-HEAs	1 M KOH + 0.5 M NaCl	$\eta_{100} = \sim 332$	72 h ~ 100 mA·cm ⁻²	This work
Fe-Ni(OH) ₂ /Ni ₃ S ₂	1 M KOH + 0.5 M NaCl	$\eta_{100} = \sim 320$	27 h ~ 100 mA·cm ⁻²	[83]
NiFe LDH@Co ₃ O ₄ /NF	1 M KOH + 0.5 M NaCl	$\eta_{100} = 330$	—	[84]
0.5Fe-NiCo ₂ O ₄ @CC	1 M KOH + 0.5 M NaCl	$\eta_{10} = 273$	—	[85]
NiCoHPi@Ni ₃ N/NF	1 M KOH + 0.5 M NaCl	$\eta_{100} = 365$	120 h ~ 200 mA·cm ⁻²	[86]
Oct-Cu ₂ O-NF	1 M KOH + 0.5 M NaCl	$\eta_{100} = 510$	—	[87]
NiMo film@NF	1 M KOH + 0.5 M NaCl	$\eta_{100} = 450$	15 h ~ 10 mA·cm ⁻²	[88]
NiCoP/NiCo-LDH@NF	1 M KOH + 0.5 M NaCl	$\eta_{50} = 350$	50 h ~ 15 mA·cm ⁻²	[89]
Ni ₃ S ₂ -MoS ₂ -Ni ₃ S ₂ @NF	1 M KOH + 0.5 M NaCl	$\eta_{100} = 330$	100 h ~ 100 mA·cm ⁻²	[90]
RuNi-Fe ₂ O ₃ /IF	1 M KOH + 0.5 M NaCl	$\eta_{100} = \sim 350$	20 h ~ 100 mA·cm ⁻²	[91]
CoSe/MoSe ₂	1 M KOH + 0.5 M NaCl	$\eta_{10} = 320$	48 h ~ 10 mA·cm ⁻²	[92]
Mo-CoPX/NF	1 M KOH + 0.5 M NaCl	$\eta_{100} = 420$	100 h ~ 10 mA·cm ⁻²	[93]
B-CoNiOOH/PANI@TiO ₂ /Ti	1 M KOH + 0.5 M NaCl	$\eta_{100} = 398$	72 h ~ 200 mA·cm ⁻²	[94]
CoCH@CFP	1 M KOH + 0.5 M NaCl	$\eta_{100} = 385$	—	[95]
MoNiFe-OH/NFF	1 M KOH	$\eta_{100} = 323$	100 h ~ 100 mA·cm ⁻²	[96]
NiFeCo-LDHs	1 M KOH	$\eta_{100} = \sim 330$	80 h ~ 100 mA·cm ⁻²	[97]
FeCoNiMnCu HEAs	1 M KOH	$\eta_{10} = 280$	40 h ~ 10 mA·cm ⁻²	[70]
(Fe _{0.25} Co _{0.61} Cu _{0.14})Se	1 M KOH	$\eta_{10} = 278$	18 h ~ 10 mA·cm ⁻²	[98]

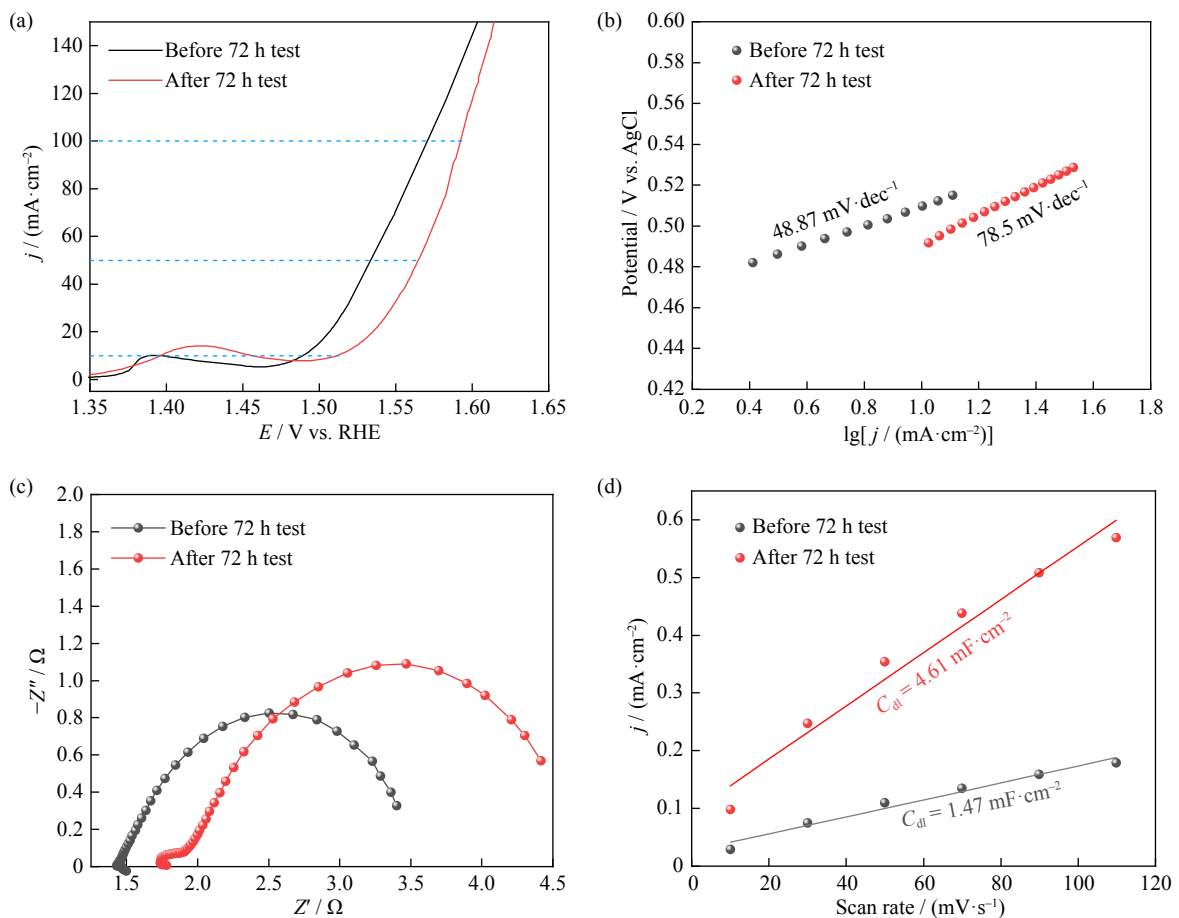


Fig. 7. Electrochemical performance in 0.5 M NaCl + 1 M KOH of the catalyst before and after the 72 h stability test: (a) LSV curves; (b) Tafel slope; (c) Nyquist plots; (d) C_{dl} values.

CoCrFeNi-LDHs-BST (Fig. 7(d)) due to its rough surface, which was caused by continual current and resulting in the exposure of additional active sites (not highly efficient active sites for OER). Fig. S7 shows that the morphology of LDHs remained unchanged after the long-term stability test, and this finding demonstrates the robustness of the interlaced sheet structure. Compared with AlCoCrFeNi-LDHs-BST (Fig. S8), no new peaks were found in the XRD pattern of AlCoCrFeNi-LDHs-AST, verifying the stable chemical compositions of AlCoCrFeNi-LDHs. XPS measurement was conducted to study the element states of AlCoCrFeNi-LDHs-AST, and all fitted peaks show nearly negligible shifts in Al 2p, Cr 2p, Fe 2p, Ni 2p, and O 1s XPS spectra (Fig. S4). The enhanced signal in the Co 2p XPS spectrum implies the oxidation of the Co element under the action of current on the electrode. Furthermore, the content of metallic ions dissolved in the electrolyte after the stability test was investigated by ICP measurement. The concentration of Co ions was too low to be considered. Notably, no significant difference was observed in the dissolution of each ion despite the lowest content of Fe in LDHs (Fig. 8). Thus, the degradation of OER electrocatalytic performance primarily originated from the collapse of highly efficient active sites, which mainly comprise Fe element.

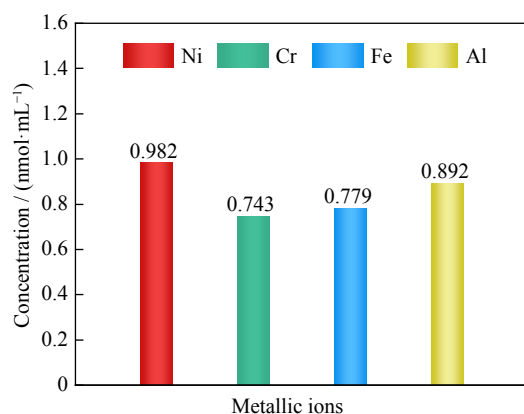


Fig. 8. Concentration of metallic ions dissolved in the electrolyte.

4. Conclusion

In summary, one-step synthesis of quinary AlCoCrFeNi-LDHs thin sheets, which were directly grown on AlCoCrFeNi-HEAs, was achieved using a facile hydrothermal method. As-formed AlCoCrFeNi-LDHs are highly porous, self-supported on the substrate, and afford a large surface area, which ensure efficient mass and charge transfer and abundant active metal sites for enhanced OER activity in alkaline seawater electrolyte. The optimal synthesis parameter of the catalyst is heated in 3 M NaOH solution for 8 h under the temperature of 150°C, which exhibits a low overpotential of 272.3 and 332 mV at 10 and 100 mA·cm⁻², respectively, and yields a small Tafel slope of 48.87 mV·dec⁻¹. In addition, the AlCoCrFeNi-LDHs catalyst presents almost no fading and a

small degradation after the first 24 and following 48 h stability test. The 2D structure, chemical composition, and chemical states were well maintained after long-term test in comparison with initial as-prepared AlCoCrFeNi-LDHs. Meanwhile, the dissolution of highly efficient catalytic sites is presumed to be the major reason for the attenuated OER activity. This facile preparation scheme of AlCoCrFeNi-LDHs represents a potential method to develop other multicomponent and non-noble metal-based LDH catalysts for large-scale seawater splitting and hydrogen production.

Acknowledgements

This work was supported by the National Natural Science Foundation of China (No. 51901018), the Young Elite Scientists Sponsorship Program by the China Association for Science and Technology (YESS, 2019QNRC001), the Natural Science Foundation of Beijing Municipality (No. 2212037), and the National Science and Technology Resources Investigation Program of China (No. 2019FY 101400).

Conflict of Interest

Bowei Zhang and Yizhong Huang are a youth editorial board member and an editorial board member for this journal respectively and were not involved in the editorial review or the decision to publish this article. The authors declare that they have no conflict of interest.

Supplementary Information

The online version contains supplementary material available at <https://doi.org/10.1007/s12613-023-2624-7>.

References

- [1] F. Yu, H.Q. Zhou, Y.F. Huang, *et al.*, High-performance bifunctional porous non-noble metal phosphide catalyst for overall water splitting, *Nat. Commun.*, 9(2018), No. 1, art. No. 2551.
- [2] K. Rennings, B. Brohmann, J. Nentwich, J. Schleich, T. Traber, and R. Wüstenhagen, *Sustainable Energy Consumption in Residential Buildings*, Springer Science, Berlin, 2012.
- [3] J.O. Abe, A.P.I. Popoola, E. Ajenifuja, and O.M. Popoola, Hydrogen energy, economy and storage: Review and recommendation, *Int. J. Hydrogen Energy*, 44(2019), No. 29, p. 15072.
- [4] C.J. Winter, Hydrogen energy—Abundant, efficient, clean: A debate over the energy-system-of-change, *Int. J. Hydrogen Energy*, 34(2009), No. 14, p. S1.
- [5] Z.P. Wu, X.F. Lu, S.Q. Zang, and X. Lou, Non-noble-metal-based electrocatalysts toward the oxygen evolution reaction, *Adv. Funct. Mater.*, 30(2020), No. 15, art. No. 1910274.
- [6] M.Y. Wang, Z. Wang, X.Z. Gong, and Z.C. Guo, The intensification technologies to water electrolysis for hydrogen production—A review, *Renewable Sustainable Energy Rev.*, 29(2014), p. 573.
- [7] S. Dresp, F. Dionigi, M. Klingenhof, and P. Strasser, Direct electrolytic splitting of seawater: Opportunities and challenges, *ACS Energy Lett.*, 4(2019), No. 4, p. 933.
- [8] S.C. Ke, R. Chen, G.H. Chen, and X.L. Ma, Mini review on

- electrocatalyst design for seawater splitting: Recent progress and perspectives, *Energy Fuels*, 35(2021), No. 16, p. 12948.
- [9] L. Yu, Q. Zhu, S.W. Song, *et al.*, Non-noble metal–nitride based electrocatalysts for high-performance alkaline seawater electrolysis, *Nat. Commun.*, 10(2019), No. 1, art. No. 5106.
- [10] F. Song, L.C. Bai, A. Moysiadou, *et al.*, Transition metal oxides as electrocatalysts for the oxygen evolution reaction in alkaline solutions: An application-inspired renaissance, *J. Am. Chem. Soc.*, 140(2018), No. 25, p. 7748.
- [11] W.M. Tong, M. Forster, F. Dionigi, *et al.*, Electrolysis of low-grade and saline surface water, *Nat. Energy*, 5(2020), No. 5, p. 367.
- [12] T. Okada, H. Abe, A. Murakami, *et al.*, A bilayer structure composed of Mg[Co–MnO₂] deposited on a Co(OH)₂ film to realize selective oxygen evolution from chloride-containing water, *Langmuir*, 36(2020), No. 19, p. 5227.
- [13] S. Gupta, M. Forster, A. Yadav, A.J. Cowan, N. Patel, and M. Patel, Highly efficient and selective metal oxy-boride electrocatalysts for oxygen evolution from alkali and saline solutions, *ACS Appl. Energy Mater.*, 3(2020), No. 8, p. 7619.
- [14] F. Dionigi, T. Reier, Z. Pawolek, M. Gliech, and P. Strasser, Design criteria, operating conditions, and nickel–iron hydroxide catalyst materials for selective seawater electrolysis, *ChemSusChem*, 9(2016), No. 9, p. 962.
- [15] G.B. Liu, Y.S. Xu, T. Yang, and L.H. Jiang, Recent advances in electrocatalysts for seawater splitting, *Nano Mater. Sci.*, 5(2023), No. 1, p. 101.
- [16] J.E. Bennett, Electrodes for generation of hydrogen and oxygen from seawater, *Int. J. Hydrogen Energy*, 5(1980), No. 4, p. 401.
- [17] J. Geng, L. Kuai, E.J. Kan, Q. Wang, and B.Y. Geng, Precious-metal-free Co–Fe–O/rGO synergetic electrocatalysts for oxygen evolution reaction by a facile hydrothermal route, *ChemSusChem*, 8(2015), No. 4, p. 659.
- [18] Y. Zhou, S.Q. Xi, X.G. Yang, and H.J. Wu, *In situ* hydrothermal growth of metallic Co₉S₈–Ni₃S₂ nanoarrays on nickel foam as bifunctional electrocatalysts for hydrogen and oxygen evolution reactions, *J. Solid State Chem.*, 270(2019), p. 398.
- [19] Z.J. Du, D.H. Xiong, S.K. Verma, *et al.*, A low temperature hydrothermal synthesis of delafossite CuCoO₂ as an efficient electrocatalyst for the oxygen evolution reaction in alkaline solutions, *Inorg. Chem. Front.*, 5(2018), No. 1, p. 183.
- [20] J.Z. Huang, J.C. Han, R. Wang, *et al.*, Improving electrocatalysts for oxygen evolution using Ni_xFe_{3–x}O₄/Ni hybrid nanostructures formed by solvothermal synthesis, *ACS Energy Lett.*, 3(2018), No. 7, p. 1698.
- [21] D.H. Youn, Y.B. Park, J.Y. Kim, G. Magesh, Y.J. Jang, and J.S. Lee, One-pot synthesis of NiFe layered double hydroxide/reduced graphene oxide composite as an efficient electrocatalyst for electrochemical and photoelectrochemical water oxidation, *J. Power Sources*, 294(2015), p. 437.
- [22] W.X. Zhu, T.S. Zhang, Y. Zhang, *et al.*, A practical-oriented NiFe-based water-oxidation catalyst enabled by ambient redox and hydrolysis co-precipitation strategy, *Appl. Catal. B*, 244(2019), p. 844.
- [23] S.M. Saha and A.K. Ganguli, FeCoNi alloy as noble metal-free electrocatalyst for oxygen evolution reaction (OER), *ChemistrySelect*, 2(2017), No. 4, p. 1630.
- [24] T.T. Liu, Y.H. Liang, Q. Liu, X.P. Sun, Y.Q. He, and A.M. Asiri, Electrodeposition of cobalt–sulfide nanosheets film as an efficient electrocatalyst for oxygen evolution reaction, *Electrochim. Commun.*, 60(2015), p. 92.
- [25] Q. Liu, S. Gu, and C.M. Li, Electrodeposition of nickel–phosphorus nanoparticles film as a Janus electrocatalyst for electro-splitting of water, *J. Power Sources*, 299(2015), p. 342.
- [26] T. Wang, W.C. Xu, and H.X. Wang, Ternary NiCoFe layered double hydroxide nanosheets synthesized by cation exchange reaction for oxygen evolution reaction, *Electrochim. Acta*, 257(2017), p. 118.
- [27] X.T. Feng, Q.Z. Jiao, H.R. Cui, *et al.*, One-pot synthesis of NiCo₂S₄ hollow spheres via sequential ion-exchange as an enhanced oxygen bifunctional electrocatalyst in alkaline solution, *ACS Appl. Mater. Interfaces*, 10(2018), No. 35, p. 29521.
- [28] J.Y. Xia, K. Huang, Z.X. Yao, *et al.*, Ternary duplex FeCoNi alloy prepared by cathode plasma electrolytic deposition as a high-efficient electrocatalyst for oxygen evolution reaction, *J. Alloys Compd.*, 891(2022), art. No. 161934.
- [29] F. Wu, Z.X. Yao, K. Huang, *et al.*, Boosting OER activity of stainless steel by cathodic plasma surface modification, *J. Mater. Res. Technol.*, 15(2021), p. 6721.
- [30] X.P. Liu, M.X. Gong, S. Deng, *et al.*, Transforming damage into benefit: Corrosion engineering enabled electrocatalysts for water splitting, *Adv. Funct. Mater.*, 31(2021), No. 11, art. No. 2009032.
- [31] H.A. Yang, L.Q. Gong, H.M. Wang, *et al.*, Preparation of nickel–iron hydroxides by microorganism corrosion for efficient oxygen evolution, *Nat. Commun.*, 11(2020), No. 1, art. No. 5075.
- [32] H. Schäfer, D.M. Chevrier, P. Zhang, *et al.*, Electro-oxidation of Ni42 steel: A highly active bifunctional electrocatalyst, *Adv. Funct. Mater.*, 26(2016), No. 35, p. 6402.
- [33] Q. Wang, Y.L. Jia, M.P. Wang, *et al.*, Synthesis of Cu₂O nanotubes with efficient photocatalytic activity by electrochemical corrosion method, *J. Phys. Chem. C*, 119(2015), No. 38, p. 22066.
- [34] B. Fei, Z.L. Chen, J.X. Liu, *et al.*, Ultrathinning nickel sulfide with modulated electron density for efficient water splitting, *Adv. Energy Mater.*, 10(2020), No. 41, art. No. 2001963.
- [35] N. Todoroki and T. Wadayama, Heterolayered Ni–Fe hydroxide/oxide nanostructures generated on a stainless-steel substrate for efficient alkaline water splitting, *ACS Appl. Mater. Interfaces*, 11(2019), No. 47, p. 44161.
- [36] H. Schäfer, S. Sadaf, L. Walder, *et al.*, Stainless steel made to rust: A robust water-splitting catalyst with benchmark characteristics, *Energy Environ. Sci.*, 8(2015), No. 9, p. 2685.
- [37] X. Shang, Z.Z. Liu, J.Q. Zhang, *et al.*, Electrochemical corrosion engineering for Ni–Fe oxides with superior activity toward water oxidation, *ACS Appl. Mater. Interfaces*, 10(2018), No. 49, p. 42217.
- [38] J. Lee, G.H. Lim, and B. Lim, Nanostructuring of metal surfaces by corrosion for efficient water splitting, *Chem. Phys. Lett.*, 644(2016), p. 51.
- [39] X.F. Ren, Y.R. Wang, A.M. Liu, Z.H. Zhang, Q.Y. Lv, and B.H. Liu, Current progress and performance improvement of Pt/C catalysts for fuel cells, *J. Mater. Chem. A*, 8(2020), No. 46, p. 24284.
- [40] Y. Yan, B.Y. Xia, B. Zhao, and X. Wang, A review on noble-metal-free bifunctional heterogeneous catalysts for overall electrochemical water splitting, *J. Mater. Chem. A*, 4(2016), No. 45, p. 17587.
- [41] S.M. Han, Q.B. Yun, S.Y. Tu, L.J. Zhu, W.B. Cao, and Q.P. Lu, Metallic ruthenium-based nanomaterials for electrocatalytic and photocatalytic hydrogen evolution, *J. Mater. Chem. A*, 7(2019), No. 43, p. 24691.
- [42] H.M. Xu, S.Q. Ci, Y.C. Ding, G.X. Wang, and Z.H. Wen, Recent advances in precious metal-free bifunctional catalysts for electrochemical conversion systems, *J. Mater. Chem. A*, 7(2019), No. 14, p. 8006.
- [43] W.S. Yan, J.T. Zhang, A.J. Lü, S.L. Lu, Y. Zhong, and M.Y. Wang, Self-supporting and hierarchically porous Ni_xFe–S/NiFe₂O₄ heterostructure as a bifunctional electrocatalyst for fluctuating overall water splitting, *Int. J. Miner. Metall. Mater.*, 29(2022), p. 1120.
- [44] Y.N. Guo, T. Park, J.W. Yi, *et al.*, Nanoarchitectonics for transition-metal-sulfide-based electrocatalysts for water splitting,

- Adv. Mater.*, 31(2019), No. 17, art. No. 1807134.
- [45] Q.B. Yun, L.X. Li, Z.N. Hu, Q. Lu, B. Chen, and H. Zhang, Layered transition metal dichalcogenide-based nanomaterials for electrochemical energy storage, *Adv. Mater.*, 32(2020), No. 1, art. No. 1903826.
- [46] H.J. Zhang, A.W. Maijenburg, X.P. Li, S.L. Schweizer, and R.B. Wehrspohn, Bifunctional heterostructured transition metal phosphides for efficient electrochemical water splitting, *Adv. Funct. Mater.*, 30(2020), No. 34, art. No. 2003261.
- [47] L.H. Liu, N. Li, J.R. Han, K.L. Yao, and H.Y. Liang, Multicomponent transition metal phosphide for oxygen evolution, *Int. J. Miner. Metall. Mater.*, 29(2022), No. 3, p. 503.
- [48] X. Peng, C.R. Pi, X.M. Zhang, S. Li, K.F. Huo, and P.K. Chu, Recent progress of transition metal nitrides for efficient electrocatalytic water splitting, *Sustainable Energy Fuels*, 3(2019), No. 2, p. 366.
- [49] W.T. Hong, M. Risch, K.A. Stoerzinger, A. Grimaud, J. Suntivich, and Y. Shao-Horn, Toward the rational design of non-precious transition metal oxides for oxygen electrocatalysis, *Energy Environ. Sci.*, 8(2015), No. 5, p. 1404.
- [50] M.S. Burke, L.J. Enman, A.S. Batchellor, S.H. Zou, and S.W. Boettcher, Oxygen evolution reaction electrocatalysis on transition metal oxides and (oxy)hydroxides: Activity trends and design principles, *Chem. Mater.*, 27(2015), No. 22, p. 7549.
- [51] K.X. Zhang and R.Q. Zou, Advanced transition metal-based OER electrocatalysts: Current status, opportunities, and challenges, *Small*, 17(2021), No. 37, art. No. 2100129.
- [52] H. Xu, H.Y. Shang, C. Wang, and Y.K. Du, Surface and interface engineering of noble-metal-free electrocatalysts for efficient overall water splitting, *Coord. Chem. Rev.*, 418(2020), art. No. 213374.
- [53] J.A. Wang, Y. Gao, H. Kong, et al., Non-precious-metal catalysts for alkaline water electrolysis: Operando characterizations, theoretical calculations, and recent advances, *Chem. Soc. Rev.*, 49(2020), No. 24, p. 9154.
- [54] G.L. Fan, F. Li, D.G. Evans, and X. Duan, Catalytic applications of layered double hydroxides: Recent advances and perspectives, *Chem. Soc. Rev.*, 43(2014), No. 20, p. 7040.
- [55] M. Xu and M. Wei, Layered double hydroxide-based catalysts: Recent advances in preparation, structure, and applications, *Adv. Funct. Mater.*, 28(2018), No. 47, art. No. 1802943.
- [56] Z.P. Xu, J. Zhang, M.O. Adebajo, H. Zhang, and C.H. Zhou, Catalytic applications of layered double hydroxides and derivatives, *Appl. Clay Sci.*, 53(2011), No. 2, p. 139.
- [57] S. Anantharaj, S.R. Ede, K. Sakthikumar, K. Karthick, S. Mishra, and S. Kundu, Recent trends and perspectives in electrochemical water splitting with an emphasis on sulfide, selenide, and phosphide catalysts of Fe, Co, and Ni: A review, *ACS Catal.*, 6(2016), No. 12, p. 8069.
- [58] M. Görlin, P. Chernev, J.F. de Araújo, et al., Oxygen evolution reaction dynamics, faradaic charge efficiency, and the active metal redox states of Ni–Fe oxide water splitting electrocatalysts, *J. Am. Chem. Soc.*, 138(2016), No. 17, p. 5603.
- [59] P. Babar, A. Lokhande, V. Karade, et al., Bifunctional 2D electrocatalysts of transition metal hydroxide nanosheet arrays for water splitting and urea electrolysis, *ACS Sustainable Chem. Eng.*, 7(2019), No. 11, p. 10035.
- [60] D.M. Jang, I.H. Kwak, E.L. Kwon, et al., Transition-metal doping of oxide nanocrystals for enhanced catalytic oxygen evolution, *J. Phys. Chem. C*, 119(2015), No. 4, p. 1921.
- [61] Y.Q. Zhang, D.D. Wang, and S.Y. Wang, High-entropy alloys for electrocatalysis: Design, characterization, and applications, *Small*, 18(2022), No. 7, art. No. 2104339.
- [62] N. Kumar Katiyar, K. Biswas, J.W. Yeh, S. Sharma, and C. Sekhar Tiwary, A perspective on the catalysis using the high entropy alloys, *Nano Energy*, 88(2021), art. No. 106261.
- [63] K. Li and W. Chen, Recent progress in high-entropy alloys for catalysts: Synthesis, applications, and prospects, *Mater. Today Energy*, 20(2021), art. No. 100638.
- [64] J. Tang, J.L. Xu, Z.G. Ye, X.B. Li, and J.M. Luo, Microwave sintered porous CoCrFeNiMo high entropy alloy as an efficient electrocatalyst for alkaline oxygen evolution reaction, *J. Mater. Sci. Technol.*, 79(2021), p. 171.
- [65] S.Q. Zhao, H.Y. Wu, R. Yin, et al., Preparation and electrocatalytic properties of (FeCrCoNiAl_{0.1})O_x high-entropy oxide and NiCo–(FeCrCoNiAl_{0.1})O_x heterojunction films, *J. Alloys Compd.*, 868(2021), art. No. 159108.
- [66] P.Y. Ma, S.C. Zhang, M.T. Zhang, et al., Hydroxylated high-entropy alloy as highly efficient catalyst for electrochemical oxygen evolution reaction, *Sci. China Mater.*, 63(2020), p. 2613.
- [67] J. Tang, J.L. Xu, Z.G. Ye, et al., Synthesis of flower-like cobalt, nickel phosphates grown on the surface of porous high entropy alloy for efficient oxygen evolution, *J. Alloys Compd.*, 885(2021), art. No. 160995.
- [68] Y.E. Xin, S.H. Li, Y.Y. Qian, et al., High-entropy alloys as a platform for catalysis: Progress, challenges, and opportunities, *ACS Catal.*, 10(2020), No. 19, p. 11280.
- [69] K. Huang, B.W. Zhang, J.S. Wu, et al., Exploring the impact of atomic lattice deformation on oxygen evolution reactions based on a sub-5 nm pure face-centred cubic high-entropy alloy electrocatalyst, *J. Mater. Chem. A*, 8(2020), No. 24, p. 11938.
- [70] K. Huang, D.D. Peng, Z.X. Yao, et al., Cathodic plasma driven self-assembly of HEAs dendrites by pure single FCC FeCoNiMnCu nanoparticles as high efficient electrocatalysts for OER, *Chem. Eng. J.*, 425(2021), art. No. 131533.
- [71] B. Huang, W.H. Xiong, Q.Q. Yang, Z.H. Yao, G.P. Zhang, and M. Zhang, Preparation, microstructure and mechanical properties of multicomponent Ni₃Al-bonded cermets, *Ceram. Int.*, 40(2014), No. 9, p. 14073.
- [72] F. Monireh and A. Nasim, NiCoFe-layered double hydroxides/MXene/N-doped carbon nanotube composite as a high performance bifunctional catalyst for oxygen electrocatalytic reactions in metal–air batteries, *J. Electroanal. Chem.*, 901(2021), art. No. 115797.
- [73] J. Yang, A.G. Baker, H.W. Liu, W.N. Martens, and R.L. Frost, Size-controllable synthesis of chromium oxyhydroxide nanomaterials using a soft chemical hydrothermal route, *J. Mater. Sci.*, 45(2010), No. 24, p. 6574.
- [74] L.M. Cao, J.W. Wang, D.C. Zhong, and T.B. Lu, Template-directed synthesis of sulphur doped NiCoFe layered double hydroxide porous nanosheets with enhanced electrocatalytic activity for the oxygen evolution reaction, *J. Mater. Chem. A*, 6(2018), No. 7, p. 3224.
- [75] D.R. Lide, eds., *CRC Handbook of Chemistry and Physics*, CRC Press, Boca Raton, 2004.
- [76] X.Z. Guo, G.Z. Liang, and A.J. Gu, Construction of nickel-doped cobalt hydroxides hexagonal nanoplates for advanced oxygen evolution electrocatalysis, *J. Colloid Interface Sci.*, 553(2019), p. 713.
- [77] Q. Zhou, Y.P. Chen, G.Q. Zhao, et al., Active-site-enriched iron-doped nickel/cobalt hydroxide nanosheets for enhanced oxygen evolution reaction, *ACS Catal.*, 8(2018), No. 6, p. 5382.
- [78] Z.L. Wang, W.J. Liu, Y.M. Hu, et al., Cr-doped CoFe layered double hydroxides: Highly efficient and robust bifunctional electrocatalyst for the oxidation of water and urea, *Appl. Catal. B*, 272(2020), art. No. 118959.
- [79] J.F. Chang, G.Z. Wang, Z.Z. Yang, et al., Dual-doping and synergism toward high-performance seawater electrolysis, *Adv. Mater.*, 33(2021), No. 33, art. No. 2101425.
- [80] X. Long, S. Xiao, Z.L. Wang, X.L. Zheng, and S.H. Yang, Co intake mediated formation of ultrathin nanosheets of transition metal LDH—An advanced electrocatalyst for oxygen evolution reaction, *Chem. Commun.*, 51(2015), No. 6, p. 1120.

- [81] X. Long, Z.L. Wang, S. Xiao, Y.M. An, and S.H. Yang, Transition metal based layered double hydroxides tailored for energy conversion and storage, *Mater. Today*, 19(2016), No. 4, p. 213.
- [82] H.M. Sun, Z.H. Yan, F.M. Liu, W.C. Xu, F.Y. Cheng, and J. Chen, Self-supported transition-metal-based electrocatalysts for hydrogen and oxygen evolution, *Adv. Mater.*, 32(2020), No. 3, art. No. 1806326.
- [83] B.H. Cui, Z. Hu, C. Liu, *et al.*, Heterogeneous lamellar-edged Fe–Ni(OH)₂/Ni₃S₂ nanoarray for efficient and stable seawater oxidation, *Nano Res.*, 14(2021), p. 1149.
- [84] C.J. Lyu, J.R. Cheng, K.L. Wu, *et al.*, Interfacial electronic structure modulation of CoP nanowires with FeP nanosheets for enhanced hydrogen evolution under alkaline water/seawater electrolytes, *Appl. Catal. B*, 317(2022), art. No. 121799.
- [85] J. Yang, Y.N. Wang, J.E. Yang, *et al.*, Quench-induced surface engineering boosts alkaline freshwater and seawater oxygen evolution reaction of porous NiCo₂O₄ nanowires, *Small*, 18(2022), No. 3, art. No. 2106187.
- [86] H. Sun, J.K. Sun, Y.Y. Song, *et al.*, Nickel–cobalt hydrogen phosphate on nickel nitride supported on nickel foam for alkaline seawater electrolysis, *ACS Appl. Mater. Interfaces*, 14(2022), No. 19, p. 22061.
- [87] H. Wang, J. Ying, Y.X. Xiao, *et al.*, Ultrafast synthesis of Cu₂O octahedrons inlaid in Ni foam for efficient alkaline water/seawater electrolysis, *Electrochem. Commun.*, 134(2022), art. No. 107177.
- [88] W.J. Yuan, Z.D. Cui, S.L. Zhu, Z.Y. Li, S.L. Wu, and Y.Q. Liang, Structure engineering of electrodeposited NiMo films for highly efficient and durable seawater splitting, *Electrochim. Acta*, 365(2021), art. No. 137366.
- [89] Y.H. Wu, Z.N. Tian, S.F. Yuan, *et al.*, Solar-driven self-powered alkaline seawater electrolysis via multifunctional earth-abundant heterostructures, *Chem. Eng. J.*, 411(2021), art. No. 128538.
- [90] Y.C. Li, X.Y. Wu, J.P. Wang, *et al.*, Sandwich structured Ni₃S₂–MoS₂–Ni₃S₂@Ni foam electrode as a stable bifunctional electrocatalyst for highly sustained overall seawater splitting, *Electrochim. Acta*, 390(2021), art. No. 138833.
- [91] T. Cui, X.J. Zhai, L.L. Guo, *et al.*, Controllable synthesis of a self-assembled ultralow Ru, Ni-doped Fe₂O₃ lily as a bifunctional electrocatalyst for large-current-density alkaline seawater electrolysis, *Chin. J. Catal.*, 43(2022), No. 8, p. 2202.
- [92] J.P. Sun, J.A. Li, Z.Z. Li, *et al.*, Modulating the electronic structure on cobalt sites by compatible heterojunction fabrication for greatly improved overall water/seawater electrolysis, *ACS Sustainable Chem. Eng.*, 10(2022), No. 30, p. 9980.
- [93] Y. Yu, J. Li, J. Luo, *et al.*, Mo-decorated cobalt phosphide nanoarrays as bifunctional electrocatalysts for efficient overall water/seawater splitting, *Mater. Today Nano*, 18(2022), art. No. 100216.
- [94] W.J. Hao, C.Y. Fu, Y.M. Wang, *et al.*, Coupling boron-modulated bimetallic oxyhydroxide with photosensitive polymer enable highly-active and ultra-stable seawater splitting, *J. Energy Chem.*, 75(2022), p. 26.
- [95] G. Li, F.S. Li, Y.L. Zhao, *et al.*, Selective electrochemical alkaline seawater oxidation catalyzed by cobalt carbonate hydroxide nanorod arrays with sequential proton-electron transfer properties, *ACS Sustainable Chem. Eng.*, 9(2021), No. 2, p. 905.
- [96] S.W. Song, Y.H. Wang, X.X. Liu, *et al.*, Synthesis of Mo-doped NiFe-phosphate hollow bird-nest architecture for efficient and stable seawater electrolysis, *Appl. Surf. Sci.*, 604(2022), art. No. 154588.
- [97] Y.S. Park, J.Y. Jeong, M.J. Jang, *et al.*, Ternary layered double hydroxide oxygen evolution reaction electrocatalyst for anion exchange membrane alkaline seawater electrolysis, *J. Energy Chem.*, 75(2022), p. 127.
- [98] X. Cao, E. Johnson, and M. Nath, Expanding multinary selenide based high-efficiency oxygen evolution electrocatalysts through combinatorial electrodeposition: Case study with Fe–Cu–Co selenides, *ACS Sustainable Chem. Eng.*, 7(2019), No. 10, p. 9588.